JOURNAL OF COMPUTATIONAL PHYSICS 83, 447–462 (1989)

Parametric Excitation of Computational Modes Inherent to Leap-Frog Scheme Applied to the Korteweg–de Vries Equation

AKIRA AOYAGI

Kyushu Industrial University, Faculty of Engineering, Matsugadai 2-327, Higashi-ku, Fukuoka-shi 813, Japan

AND

KANJI ABE

University of Tokyo, College of Arts and Sciences, Komaba 3-8-1, Meguro-ku, Tokyo 153, Japan

Received October 21, 1987; revised September 9, 1988

The numerical instability in the usage of the leap-frog scheme applied to the Korteweg–de Vries equation is studied. The leap-frog scheme generates computational modes which are not included in the original partial differential equation. It is shown that the numerical instability comes from the parametric excitation of the computational modes by physical waves. A method to suppress the computational modes is given. The method enables us to make long-time integration of the Korteweg–de Vries equation, even if the amplitude of wave is large.

1. INTRODUCTION

The numerical solution to a nonlinear partial differential equation by finite difference methods often exhibits nonlinear instability, even though linear stability conditions are satisfied. The nonlinear instability in finite difference methods has been studied from several points of view [1–5].

When the partial differential equation contains the time derivative, one of the natural ways to approximate the time derivative is to use the leap-frog scheme. The leap-frog scheme generates computational modes as well as physical modes in the numerical solution [6, 7]. The physical modes converge to the solution of the original partial differential equation when the temporal increment approachs zero, while the computational modes are unphysical modes which are not contained in the exact solution. In this paper we study interactions of the computational modes with the physical modes and show that the computational modes are parametrically excited by the physical modes.

0021-9991/89 $3.00

As a typical example noted above, we apply the leap-frog scheme to the Korteweg–de Vries equation

$$\frac{\partial u}{\partial t}+u\frac{\partial u}{\partial x}+\mu\frac{\partial^3 u}{\partial x^3}=0, \tag{1.1}$$

where μ is constant. When $|u|$ is large, the numerical solution of Eq. (1.1) shows an unphysical oscillation in the course of time, whose amplitude suddenly increases without bound. This destroys the time integration of the Korteweg–de Vries equation (1.1). We will show that the growing unphysical oscillation comes from the parametric excitation of the computational modes by the physical modes. The reason for the growing unphysical oscillation, therefore, is essentially different from those of Briggs *et al.* [6] and Hsia *et al.* [8] which have been explained on the basis of a weak nonlinear instability.

On the basis of the results theoretically clarified above, we also propose a practical method to suppress the growth of the unphysical oscillation. The method enables us to make long-time integration of the Korteweg–de Vries equation (1.1), even if $|u|$ is large.

2. Numerical Solution by the Leap-Frog Scheme

We solve Eq. (1.1) under the periodic boundary condition

$$u(x, t)=u(x+2, t), \tag{2.1}$$

and the intial condition

$$u(x, 0)=2\varepsilon_K\cos(\pi Kx), \tag{2.2}$$

where ε_K is constant and K is a positive integer. We use the Zabusky–Kruskal scheme [9]

$$u_j^{n+1}=u_j^{n-1}-\frac{\Delta t}{3\Delta x}(u_{j+1}^n+u_j^n+u_{j-1}^n)(u_{j+1}^n-u_{j-1}^n)$$

$$-\mu\frac{\Delta t}{\Delta x^3}(u_{j+2}^n-2u_{j+1}^n+2u_{j-1}^n-u_{j-2}^n), \tag{2.3}$$

where $u_j^n\equiv u(x=j\Delta x,\ t=n\Delta t)$, Δx is the spatial increment, and Δt is the temporal increment. Initial condition (2.2) becomes

$$u_j^0=2\varepsilon_K\cos(\pi Kj\,\Delta x). \tag{2.4}$$

In order to obtain the linear stability condition, we replace $(u_{j+1}^n+u_j^n+u_{j-1}^n)/3$

in the second term of the right-hand side of Eq. (2.3) by a constant c, and use the discrete Fourier transformation

$$u_j^n = \sum_{k=-J}^{J-1} U_k^n \exp\left(\frac{i\pi kj}{J}\right), \tag{2.5}$$

where $2J\,\Delta x = 2$. The condition that u_j^n is real leads to $U_{-k}^n = U_k^{n*}$, where $*$ denotes complex conjugate number. Thus we obtain the linear difference equation for U_k^n as

$$U_k^{n+1} - 2i\,\Delta t\left[\omega_k - \frac{c}{\Delta x}\sin(\pi k\,\Delta x)\right] U_k^n - U_k^{n-1} = 0, \tag{2.6}$$

where

$$\omega_k \equiv \frac{2\mu}{\Delta x^3}\sin(\pi k\,\Delta x)[1-\cos(\pi k\,\Delta x)]. \tag{2.7}$$

If we put $U_k^n \propto \exp(in\theta_k)$, the linear stability condition is given from

$$\sin\theta_k = \Delta t\left[\omega_k - \frac{c}{\Delta x}\sin(\pi k\,\Delta x)\right]. \tag{2.8}$$

The linear stability is assured if

$$\frac{\Delta t}{\Delta x}\left(|c| + \frac{4\mu}{\Delta x^2}\right) \leqslant 1. \tag{2.9}$$

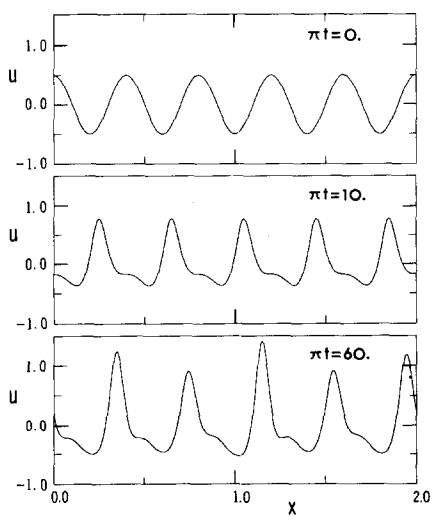

FIG. 1. Numerical solutions based on Eq. (2.3). $\mu = 0.022^2$, $\pi\,\Delta t = 5\times10^{-4}$, $\Delta x = 2/200$. $K = 5$ and $\varepsilon_K = 0.25$ in Eq. (2.4).

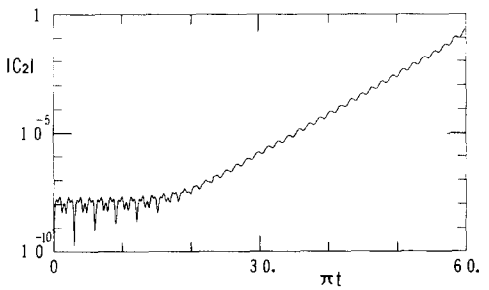

FIG. 2. Invariant C_2 for Fig. 1 as a function of time. C_2 is defined by Eq. (2.10).

We make numerical computations based on Eq. (2.3), putting $\mu = 0.022^2$, $K = 5$, $\varepsilon_K = 0.25$, $\Delta t = 5 \times 10^{-4}/\pi$, and $\Delta x = 2/200$. The Δt and Δx satisfy the linear stability condition (2.9), as long as $|c| \simeq 1$. The inverse scattering method [10] and the initial condition (2.2) give the number of solitons. The condition noted above leads to two solitons in the fundamental wave length ($2/5 = 0.4$). From the paper by Abe and Satofuka [11], the near-recurrence time is equal to $187/\pi$. Figure 1 gives the numerical solution of $u(x, t)$. We can see that two solitons appear in a fundamental wave length of 0.4 as expected, and at the time of $\pi t = 60$, however, the heights of higher solitons becomes different due to some numerical instability. The Korteweg–de Vries equation (1.1) has the conservation relation

$$C_2 \equiv \int_0^2 u(x, t)^2 \, dx - 4\varepsilon_K^2 = 0. \tag{2.10}$$

Figure 2 gives the value of $|C_2|$ as a function of time t. From the figure we see the failure of the Zabusky–Kruskal scheme (2.3) for large t.

3. PHYSICAL AND COMPUTATIONAL MODES

When the absolute value of the right-hand side of Eq. (2.8) is less than unity, we have two solutions of θ_k. If one is expressed by θ_k, the other is equal to $\pi - \theta_k$. Since $\exp[in(\pi - \theta_k)] = (-1)^n \exp(-in\theta_k)$, the solution of Eq. (2.6) is given by

$$U_k^n = V_k \exp(in\theta_k) + (-1)^n W_k \exp(-in\theta_k), \tag{3.1}$$

where V_k and W_k are independent of n. The first and the second modes represent the physical and the computational modes, respectively. The computational modes change their signs at each time step. In view of Eq. (3.1) we may approximate the nonlinear solution of U_k^n by

$$U_k^n = V_k^n + (-1)^n W_k^n. \tag{3.2}$$

We call V_k^n and W_k^n the nonlinear physical and computational modes, respectively.

When the amplitude of a wave is small, V_k^n and W_k^n reduce to linear solutions, or $V_k^n \to V_k \exp(in\theta_k)$ and $W_k^n \to W_k \exp(-in\theta_k)$.

We show a method of obtaining the physical modes V_k^n and the computational modes W_k^n from u_j^n and u_j^{n-1} which are determined through the leap-frog scheme (2.3). Substituting Eq. (3.2) into Eq. (2.5) we obtain

$$u_j^n = v_j^n + (-1)^n w_j^n, \tag{3.3}$$

where

$$\begin{pmatrix} v_j^n \\ w_j^n \end{pmatrix} = \sum_{k=-J}^{J-1} \begin{pmatrix} V_k^n \\ W_k^n \end{pmatrix} \exp\left(\frac{i\pi kj}{J}\right). \tag{3.4}$$
$$\tag{3.5}$$

In view of Eq. (3.3) we can write

$$u_j^{n-1} = v_j^{n-1} - (-1)^n w_j^{n-1}. \tag{3.6}$$

If we put $(u_j^{n+1} - u_j^{n-1})/(2\,\Delta t) = \partial u_j/\partial t$, Eq. (2.3) becomes

$$\frac{\partial u_j}{\partial t} = -\frac{1}{6\,\Delta x}(u_{j+1} + u_j + u_{j-1})(u_{j+1} - u_{j-1})$$
$$-\frac{\mu}{2\,\Delta x^3}(u_{j+2} - 2u_{j+1} + 2u_{j-1} - u_{j-2}), \tag{3.7}$$

where u_j is regarded as a function of continuous time t. We integrate Eq. (3.7) from $(n-1)\,\Delta t$ to $n\,\Delta t$ by the Runge–Kutta scheme using u_j^{n-1} as starting values to obtain u_j $(t = n\,\Delta t)$. Since the Runge–Kutta scheme is a single-step method, all modes of u_j^{n-1} in Eq. (3.6) are advanced with no such oscillation in time as the computational modes. Therefore u_j $(t = n\,\Delta t)$ may be expressed as

$$u_j(t = n\,\Delta t) = v_j^n - (-1)^n w_j^n, \tag{3.8}$$

where we have ignored the higher order errors incurred by the use of the Runge–Kutta scheme instead of the leap-frog scheme. Then from Eqs. (3.3) and (3.8) we obtain

$$v_j^n = [u_j^n + u_j(t = n\,\Delta t)]/2, \tag{3.9}$$
$$w_j^n = [u_j^n - u_j(t = n\,\Delta t)](-1)^n/2, \tag{3.10}$$

where u_j $(t = n\,\Delta t)$ is the solution by the Runge–Kutta scheme. Figure 3 is the schematic graph for u_j $(t = n\Delta t)$. The Fourier spectra V_k^n and W_k^n corresponding to v_j^n and w_j^n are given by the inverse transformation of Eqs. (3.4) and (3.5) as

$$\begin{pmatrix} V_k^n \\ W_k^n \end{pmatrix} = \frac{1}{2J} \sum_{j=0}^{2J-1} \begin{pmatrix} v_j^n \\ w_j^n \end{pmatrix} \exp\left(-\frac{i\pi kj}{J}\right). \tag{3.11}$$
$$\tag{3.12}$$

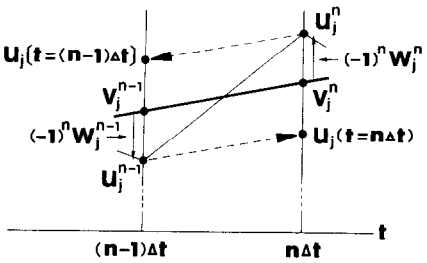

FIG. 3. Schematic graph of physical modes $v_j^{n,n-1}$ and computational modes $w_j^{n,n-1}$. $u_j^{n,n-1}$: leap-frog solutions. $u_j(t=n\,\Delta t)$, $u_j[t=(n-1)\,\Delta t]$: Runge–Kutta solutions.

Thus we obtain separately the physical and the computational modes from the numerical solution.

Figures 4 give the temporal developments of the fundamental physical mode $V_{K=5}^n$ and its second high harmonics $V_{2K=10}^n$, which correspond to the numerical solution shown in Fig. 1. From Figs. 4 it turns out that we can express V_K^n and V_{2K}^n as the sums of a low frequency wave and a high frequency wave, i.e.,

$$V_K^n = V_{K,\mathrm{lf}} \exp(in\,\Delta t \Omega_{K,\mathrm{lf}}) + V_{K,\mathrm{hf}} \exp(in\,\Delta t \Omega_{K,\mathrm{hf}}), \tag{3.13}$$

$$V_{2K}^n = V_{2K,\mathrm{lf}} \exp(in\,\Delta t \Omega_{2K,\mathrm{lf}}) + V_{2K,\mathrm{hf}} \exp(in\,\Delta t \Omega_{2K,\mathrm{hf}}), \tag{3.14}$$

where the subscripts lf and hf mean the low and high frequencies, respectively. We

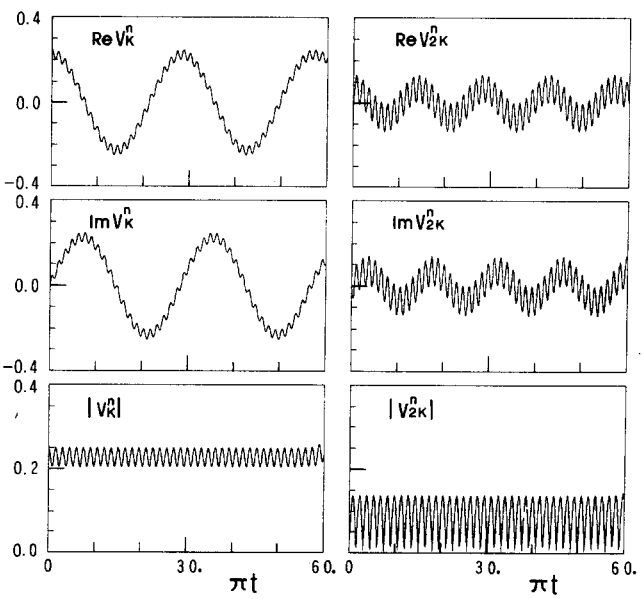

FIG. 4. The fundamental and the second high harmonics of physical modes corresponding to Fig. 1. V_K^n and V_{2K}^n are defined by Eq. (3.11).

TABLE I

Comparison between Experiment and Theory

	Experiment	Theory
$\pi\,\Delta t$	5×10^{-4}	5×10^{-4}
Δx	2/200	2/200
$V_{K,\mathrm{lf}}$	0.23	0.231
$V_{2K,\mathrm{lf}}$	7.0×10^{-2}	6.27×10^{-2}
$\Omega_{K,\mathrm{lf}}$	0.70	0.724
$\Omega_{2K,\mathrm{lf}}$	1.4	1.45
$V_{K,\mathrm{hf}}$	2.3×10^{-2}	2.16×10^{-2}
$V_{2K,\mathrm{hf}}$	7.0×10^{-2}	6.27×10^{-2}
$\Omega_{K,\mathrm{hf}}$	13.0	16.2
$\Omega_{2K,\mathrm{hf}}$	14.5	16.9
ω_K		1.86
ω_{2K}		14.6
$\lambda_{K,K}$		31.0
$\lambda_{2K,-K}$		15.5
s_1		2.27
s_2		−13.2
$\lvert s_1/s_2\rvert$		0.17

Note. $K=5$, $\varepsilon_K=0.25$.

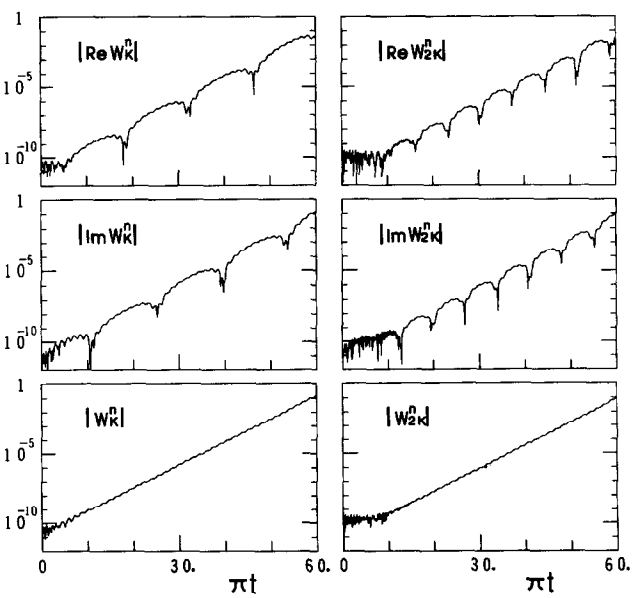

FIG. 5. The fundamental and the second high harmonics of computational modes coprresponding to Fig. 1. W^n_K and W^n_{2K} are defined by Eq. (3.12).

TABLE II

Diagram of Physical and Computational Modes

	Total	Physical modes		Computational modes	
x-space	u_j^n	v_j^n		w_j^n	
k-space	U_k^n	V_k^n		W_k^n	
		l.f.	h.f.	l.f.	h.f.
		$V_{K,\mathrm{lf}}$, $\Omega_{K,\mathrm{lf}}$ $V_{2K,\mathrm{lf}}$, $\Omega_{2K,\mathrm{lf}}$	$V_{K,\mathrm{hf}}$, $\Omega_{K,\mathrm{hf}}$ $V_{2K,\mathrm{hf}}$, $\Omega_{2K,\mathrm{hf}}$	$\Omega_{K,\mathrm{lf}}$ $\Omega_{2K,\mathrm{lf}}$	$\Omega_{K,\mathrm{hf}}$ $\Omega_{2K,\mathrm{hf}}$

Note. $u_j^n = v_j^n + (-1)^n w_j^n$, $U_k^n = V_k^n + (-1)^n W_k^n$. The captial K appears in the initial condition: $u_j^0 = v_j^0 = 2\varepsilon_K \cos(\pi K j \Delta x)$ or $U_k^0 = V_k^0 = (\delta_{k,K} + \delta_{k,-K})\varepsilon_K$.

evaluate by curve fitting the values of $V_{K,\mathrm{lf}}$, $\Omega_{K,\mathrm{lf}}$, $V_{2K,\mathrm{lf}}$, $\Omega_{2K,\mathrm{lf}}$, $V_{K,\mathrm{hf}}$, $\Omega_{K,\mathrm{hf}}$, $V_{2K,\mathrm{hf}}$ and $\Omega_{2K,\mathrm{hf}}$ from V_K^n and V_{2K}^n given in Figs. 4. The resulting $V_{K,\mathrm{lf}}$ etc. are tabulated in the left column of Table I.

Figures 5 give the temporal developments of the fundamental computational mode $W_{K=5}^n$ and its second high harmonics $W_{2K=10}^n$ associated with the physical modes shown in Figs. 4. From these figures we can put

$$|W_{K,2K}^n| \propto \exp(\gamma n \Delta t),$$

where γ is the growth rate independent of K or $2K$. The curve fitting gives $\gamma = 1.18$. The precise examination of Figs. 5 reveals that W_K^n consists of a low frequency oscillation and a high frequency oscillation, and the frequencies of the former and the latter oscillations are equal to $\Omega_{K,\mathrm{lf}}$ and $\Omega_{K,\mathrm{hf}}$ for the physical mode V_K^n given by Eq. (3.13). The same situation is found for W_{2K}^n also. Table II summarizes the physical and the computational modes. Figures 6 give the temporal developments

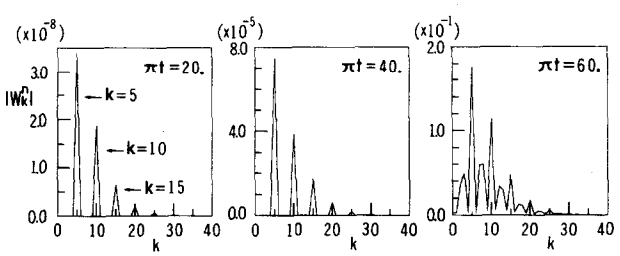

FIG. 6. Time development of the Fourier spectrum of computational modes corresponding to Fig. 1.

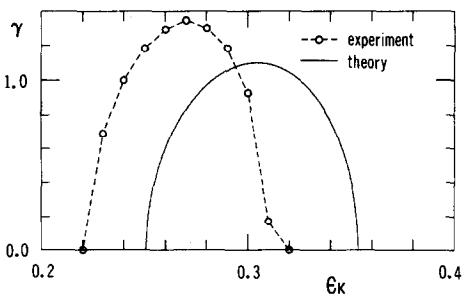

FIG. 7. The growth rate γ of computational modes as a function of the amplitude ε_K of initial wave. $K=5$. γ is defined in Eqs. (5.6) and (5.7).

of the computational modes $W^n_{k\leqslant 40}$. From these figures we see that the fundamental computational mode W^n_K and its second high harmonics W^n_{2K} dominate over the other modes.

We here emphasize that the failure of the Zabusky–Kruskal scheme (2.3), as shown in Fig. 2, comes from the growth of computational modes W^n_k (or w^n_j). We made the numerical integrations based on Eq. (2.3) for various values of the amplitude ε_K in Eq. (2.4), fixing $K=5$. The broken line in Fig. 7 gives the growth rate γ of the computational modes as a function of $\varepsilon_{K=5}$. It is interesting that the computational modes are unstable only if $0.22\leqslant\varepsilon_{K=5}\leqslant 0.32$. The solid line in Fig. 7 will be explained later.

We also made the numerical computations based on Eq. (2.3) putting $K=4$ or 6 in Eq. (2.4). We varied the values of $\varepsilon_{K=4}$ or $\varepsilon_{K=6}$. The growth rate γ of the computational modes for $K=4$ as a function of $\varepsilon_{K=4}$ is given by the broken line in Fig. 8. The γ for $K=6$ also is given in Fig. 8.

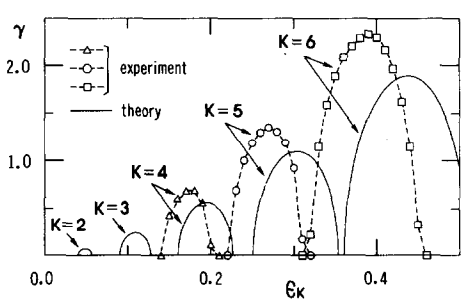

FIG. 8. The growth rate γ of computational modes for $K=2$, 3, 4, 5, or 6. Results for $K=5$ are the same as those in Fig. 7.

4. Analysis of Physical Modes

As seen from Figs. 4 and 5, at the early stage of the numerical instability, the amplitudes of computational modes are small compared to those of physical modes, or

$$|W_k^n| \ll |V_k^n|. \tag{4.1}$$

We substitute Eq. (3.2) into Eq. (2.5), and substitute Eq. (2.5) into Eq. (2.3). If we consider the inequality (4.1), we obtain

$$V_k^{n+1} - 2i\,\Delta t\omega_k V_k^n - V_k^{n-1} = -i\,\Delta t \sum_{\substack{k',k'' \\ [k'+k'']=k}} \lambda_{k',k''} V_{k'}^n V_{k''}^n, \tag{4.2}$$

and

$$W_k^{n+1} + 2i\,\Delta t\omega_k W_k^n - W_k^{n-1} = 2i\,\Delta t \sum_{\substack{k',k'' \\ [k'+k'']=k}} \lambda_{k',k''} V_{k'}^n W_{k''}^n, \tag{4.3}$$

where ω_k has been defined by Eq. (2.7) and

$$\lambda_{k',k''} \equiv \frac{1}{3\,\Delta x}\{2\sin[\pi(k'+k'')\,\Delta x] + \sin(\pi k'\,\Delta x) + \sin(\pi k''\,\Delta x)\}.$$

The brackets [ ] in Eqs. (4.2) and (4.3) are defined by

$$[l] \equiv \begin{cases} l & (-J \leqslant l \leqslant J-1), \\ l-2J & (l > J-1), \\ l+2J & (l < -J). \end{cases}$$

Equations (4.2) and (4.3) mean that the time development of the physical modes V_k^n is independent of the computational modes W_k^n, while the computational modes are parametrically coupled with the physical modes. The initial condition for V_k^n is given by Eqs. (2.4) and (3.11) as

$$V_k^0 = (\delta_{k,K} + \delta_{k,-K})\varepsilon_K,$$

where $\delta_{k,l}$ denotes the Kronecker delta. Since $V_0^0 = 0$ and $\lambda_{k,-k} = 0$, Eq. (4.2) leads us to $V_0^n = 0$. The right-hand side of Eq. (4.2) generates the higher harmonics $V_{\pm 2K}^n$, $V_{\pm 3K}^n$, etc. If ε_K is not so large, we may put $|V_{\pm K}^n| \gg |V_{\pm 2K}^n| \gg |V_{\pm 3K}^n|$..., so that we only take into account $V_{\pm K}^n$ and $V_{\pm 2K}^n$. Then Eq. (4.2) reduces to

$$V_K^{n+1} - 2i\,\Delta t\omega_K V_K^n - V_K^{n-1} = -2i\,\Delta t\lambda_{2K,-K} V_{2K}^n V_K^{n*}, \tag{4.4}$$

$$V_{2K}^{n+1} - 2i\,\Delta t\omega_{2K} V_{2K}^n - V_{2K}^{n-1} = -i\,\Delta t\lambda_{K,K}(V_K^n)^2. \tag{4.5}$$

In order to obtain approximate solutions to Eqs. (4.4) and (4.5), we regard n as continuous quantity and write Eqs. (4.4) and (4.5) in forms of differential equations

$$\left(\frac{1}{\Delta t}\frac{\partial}{\partial n} - i\omega_K\right) V_K^n = -i\lambda_{2K,-K} V_{2K}^n V_K^{n*}, \tag{4.6}$$

$$\left(\frac{1}{\Delta t}\frac{\partial}{\partial n} - i\omega_{2K}\right) V_{2K}^n = -\frac{1}{2} i\lambda_{K,K}(V_K^n)^2. \tag{4.7}$$

Equations (4.6) and (4.7) give the conservation relation

$$\tfrac{1}{2}\lambda_{K,K}|V_K^n|^2 + \lambda_{2K,-K}|V_{2K}^n|^2 = \text{const} \qquad \text{(independent of } n\text{)}.$$

If $\Delta x \ll 1$, then $\lambda_{K,K} \simeq \lambda_{2K,-K} \simeq \pi K$. Considering that $|V_{2K}^n|^2 \ll |V_K^n|^2$, we may put

$$|V_K^n|^2 = \text{const}, \tag{4.8}$$

which may be assured by Figs. 4.

If we multiply Eq. (4.6) by V_K^n and use Eq. (4.8), Eqs. (4.6) and (4.7) reduce to simultaneous linear differential equations for $(V_K^n)^2$ and V_{2K}^n. We can solve these equations analytically to obtain

$$V_K^n = \left(\frac{s_2}{s_2 - s_1}\right)^{1/2} \varepsilon_K \exp\left[\frac{1}{2} i(\omega_{2K} + s_2) n\,\Delta t\right] \times \left\{1 - \frac{s_1}{s_2}\exp[i(s_1 - s_2) n\,\Delta t]\right\}^{1/2}, \tag{4.9}$$

$$V_{2K}^n = \frac{\lambda_{K,K}}{2(s_1 - s_2)} \varepsilon_K^2 \{\exp[i(\omega_{2K} + s_2) n\,\Delta t] - \exp[i(\omega_{2K} + s_1) n\,\Delta t]\}, \tag{4.10}$$

where

$$s_1 \equiv (2\omega_K - \omega_{2K} + D^{1/2})/2, \qquad s_2 \equiv (2\omega_K - \omega_{2K} - D^{1/2})/2, \tag{4.11}$$

$$D \equiv (2\omega_K - \omega_{2K})^2 + 4\lambda_{K,K}\lambda_{2K,-K}\varepsilon_K^2.$$

The right column of Table I gives the values of ω_K, ω_{2K}, $\lambda_{K,K}$, $\lambda_{2K,-K}$, s_1, and s_2 when $K = 5$ and $\varepsilon_K = 0.25$.

If we put $\omega_K \simeq \mu(\pi K)^3$, $\omega_{2K} \simeq 8\mu(\pi K)^3$, $\lambda_{k',k''} \simeq 3\pi(k' + k'')\,\Delta x$, we obtain from Eqs. (4.11)

$$\left|\frac{s_1}{s_2}\right| \simeq \frac{\varepsilon_K^2}{18\mu^2(\pi K)^4 + \varepsilon_K^2},$$

so that $|s_1/s_2| \ll 1$ if $|\varepsilon_K| \ll 1$. Assuming $|s_1/s_2| \ll 1$, we expand Eq. (4.9) as

$$V_K^n = \left(1 + \frac{s_1}{2s_2}\right) \varepsilon_K \exp\left[\frac{1}{2} i(\omega_{2K} + s_2) n\,\Delta t\right] - \frac{s_1}{2s_2} \varepsilon_K \exp\left[\frac{1}{2} i(\omega_{2K} + 2s_1 - s_2) n\,\Delta t\right]. \tag{4.12}$$

We can give approximate expressions of the four frequencies in Eqs. (4.12) and (4.10) as

$$\tfrac{1}{2}(\omega_{2K} + s_2) \simeq \tfrac{1}{2}\omega_K, \qquad \tfrac{1}{2}(\omega_{2K} + 2s_1 - s_2) \simeq 7\omega_K,$$
$$\omega_{2K} + s_2 \simeq \omega_K, \qquad \omega_{2K} + s_1 \simeq 8\omega_K.$$

Thus we see that V_K^n and V_{2K}^n consist of two oscillations with low and high frequencies. Comparing Eq. (3.13) with Eq. (4.12), we can put

$$V_{K,\mathrm{lf}} = \left(1 + \frac{s_1}{2s_2}\right) \varepsilon_K, \qquad \Omega_{K,\mathrm{lf}} = (\omega_{2K} + s_2)/2,$$
$$V_{K,\mathrm{hf}} = -\frac{s_1}{2s_2} \varepsilon_K, \qquad \Omega_{K,\mathrm{hf}} = (\omega_{2K} + 2s_1 - s_2)/2.$$

Comparing Eq. (3.14) with Eq. (4.10), we can put

$$V_{2K,\mathrm{lf}} = -V_{2K,\mathrm{hf}} = \frac{\lambda_{K,K}}{2(s_1 - s_2)} \varepsilon_K^2,$$
$$\Omega_{2K,\mathrm{lf}} = \omega_{2K} + s_2, \qquad \Omega_{2K,\mathrm{hf}} = \omega_{2K} + s_1.$$

The right column of Table I gives the values of $V_{K,\mathrm{lf}}$ etc. for $K = 5$ and $\varepsilon_K = 0.25$. We see a good agreement between experiment and theory.

5. Parametric Excitation of Computational Modes

In view of Fig. 6, we consider only W_K^n and W_{2K}^n. Then Eq. (4.3) reduces to

$$W_K^{n+1} + 2i\,\Delta t \omega_K W_K^n - W_K^{n-1} = 2i\,\Delta t \lambda_{2K,-K}(V_{2K}^n W_K^{n*} + V_K^{n*} W_{2K}^n), \tag{5.1}$$
$$W_{2K}^{n+1} + 2i\,\Delta t \omega_{2K} W_{2K}^n - W_{2K}^{n-1} = 2i\,\Delta t \lambda_{K,K} V_K^n W_K^n. \tag{5.2}$$

If we regard n as a continuous quantity, we can write the left-hand side of Eqs. (5.1) and (5.2) as

$$\left(\frac{1}{\Delta t}\frac{\partial}{\partial n} + i\omega_K\right) W_K^n, \qquad \left(\frac{1}{\Delta t}\frac{\partial}{\partial n} + i\omega_{2K}\right) W_{2K}^n,$$

so that the natural frequencies of W_K^n and W_{2K}^n are $-\omega_K$ and $-\omega_{2K}$, respectively. Thus phase rotations of W_K^n and W_{2K}^n are in the opposite direction to those of the high frequency parts of the physical modes. Therefore, we can not expect parametric coupling between the computational modes and the high frequency parts of the physical modes. We consider only the low frequency parts of the physical modes given in Eqs. (4.9) and (4.10) as the pumping modes

$$V_K^n = V_K \exp(in\,\Delta t\Omega_K), \tag{5.3}$$

$$V_{2K}^n = V_{2K} \exp(i2n\,\Delta t\Omega_K), \tag{5.4}$$

where

$$V_K \equiv \left(\frac{s_2}{s_2 - s_1}\right)^{1/2} \varepsilon_K, \qquad V_{2K} \equiv \frac{\lambda_{K,K}}{2(s_1 - s_2)} \varepsilon_K^2, \qquad \Omega_K \equiv (\omega_{2K} + s_2)/2. \tag{5.5}$$

In order to solve Eqs. (5.1) and (5.2) we put

$$W_K^n = W_K \exp[(i\Omega_K + \gamma)n\,\Delta t], \tag{5.6}$$

$$W_{2K}^n = W_{2K} \exp[(i2\Omega_K + \gamma)n\,\Delta t]. \tag{5.7}$$

From Figs. 4 and 5 we have assumed that the frequencies of W_K^n and W_{2K}^n are equal to those of V_K^n and V_{2K}^n, respectively. This assumption is recognizable as the condition of frequency locking for the parametric excitation, viz. te frequencies of the parametrically excited waves are determined by the modulation frequencies rather than by the natural frequencies. The positive γ corresponds to the parametric excitation of the computational modes.

We substitute Eqs. (5.3), (5.4), (5.6), and (5.7) into Eqs. (5.1) and (5.2), and approximate $\exp[\pm(i\Omega_K + \gamma)\,\Delta t] \simeq 1 \pm (i\Omega_K + \gamma)\,\Delta t$, assuming $\Delta t \ll 1$. Then we obtain

$$(-i\gamma + \Omega_K + \omega_K) W_K + \lambda_{2K,-K}(V_{2K} W_K^* + V_K^* W_{2K}) = 0, \tag{5.8}$$

$$(-i\gamma + 2\Omega_K + \omega_{2K}) W_{2K} - \lambda_{K,K} V_K W_K = 0. \tag{5.9}$$

Equations (5.8) and (5.9) and their complex conjugate equations constitute the homogeneous algebraic equations for W_K, W_K^*, W_{2K}, and W_{2K}^*, whose coefficients contain V_K, V_K^*, V_{2K}, and V_{2K}^*. The condition that the determinant of the coefficient matrix is equal to zero leads to

$$\gamma^4 + c_1\gamma^2 + c_2 = 0,$$

where

$$c_1 \equiv (\Omega_K + \omega_K)^2 + (2\Omega_K + \omega_{2K})^2 + 2\lambda_{2K,-K}\lambda_{K,K}|V_K|^2 - \lambda_{2K,-K}^2|V_{2K}|^2,$$
$$c_2 \equiv [(\Omega_K + \omega_K)(2\Omega_K + \omega_{2K}) - \lambda_{2K,-K}\lambda_{K,K}|V_K|^2]^2 - (2\Omega_K + \omega_{2K})^2 \lambda_{2K,-K}^2 |V_{2K}|^2.$$

Since $c_1 > 0$, the condition $\gamma > 0$ is satisfied when $c_2 < 0$. The growth rate γ is then given by

$$\gamma = \frac{1}{\sqrt{2}} [(c_1^2 - 4c_2)^{1/2} - c_1]^{1/2}.$$

We calculated γ as a function of ε_K, fixing $K = 5$. The solid line in Fig. 7 gives γ obtained thus.

We also calculated γ as a function of ε_K, fixing $K = 2$, 3, 4, or 6. The solid lines in Fig. 8 give γ obtained thus. If we shift the theoretical curves to the left, we see a good agreement between experiment and theory.

6. Suppression of Computational Modes

In this section we propose a method to suppress the growth of computational modes. Without this method we fail to make long-time integration based on the leap-frog scheme, as shown in Fig. 2. We eliminate the computational modes at some time step.

In Section 3 we have decomposed u_j^n into the physical modes v_j^n and the computational modes w_j^n. In order to obtain u_j^{n+1} including no computational modes through the leap-frog scheme, we need u_j^n and u_j^{n-1} which include no computational modes. We replace u_j^n by v_j^n and u_j^{n-1} by v_j^{n-1} at some time step. To obtain v_j^{n-1} we integrate Eq. (3.7) in the reverse time direction by the Runge–Kutta scheme, starting from u_j^n obtained by the leap-frog scheme. The Runge–Kutta scheme yields no such oscillation in time as the computational modes, so that $u_j[t = (n-1)\,\Delta t]$ obtained by the Runge–Kutta scheme may be written, in view of Eq. (3.3), as

$$u_j[t = (n-1)\,\Delta t] = v_j^{n-1} + (-1)^n w_j^{n-1}, \tag{6.1}$$

instead of the right-hand side of Eq. (3.6). Figure 3 gives the schematic graph for $u_j[t = (n-1)\,\Delta t]$. Equations (3.6) and (6.1) give

$$v_j^{n-1} = \{u_j^{n-1} + u_j[t = (n-1)\,\Delta t]\}/2.$$

The v_j^{n-1} includes no computational modes. We summarize the algorithm as

$$u_j^n \to \{u_j^n + u_j(t = n\,\Delta t)\}/2,$$
$$u_j^{n-1} \to \{u_j^{n-1} + u_j[t = (n-1)\,\Delta t]\}/2,$$

where u_j^n and u_j^{n-1} are determined by the leap-frog scheme, $u_j(t=n\,\Delta t)$ is determined from u_j^{n-1} by the use of the Runge–Kutta scheme, and $u_j[t=(n-1)\,\Delta t]$ is determined from u_j^n by the use of the Runge–Kutta scheme.

We apply this method to the problem shown in Figs. 1 and 2. Figure 9 shows the results when the computational modes are eliminated at every 24,000 time steps. We see that $|W_{K=5}^n| < 10^{-8}$ and $|C_2| < 10^{-7}$ for all n. The Korteweg–de Vries equation (1.1) has conservation relations

$$C_1 \equiv \int_0^2 u(x, t)\, dx = 0,$$

$$C_3 \equiv \int_0^2 \left[\frac{1}{3}u^3 - \mu\left(\frac{\partial u}{\partial x}\right)^2\right] dx + \mu(2\pi K\varepsilon_K)^2 = 0,$$

as well as Eq. (2.10). The values of $|C_1|$ and $|C_3|$ remain less than 10^{-13} and 10^{-3}, respectively, for all n.

Zabusky [12] recognized that the leap-frog scheme (2.3) was subject to the numerical instability. To suppress the instability he introduced the temporal smoothing algorithm in which u_j^n and u_j^{n-1} were replaced by $(u_j^{n+1} + 2u_j^n + u_j^{n-1})/4$ and $(u_j^n + 2u_j^{n-1} + u_j^{n-2})/4$, respectively, at some time steps. We also applied this second-order smoother to the problem in this paper. Using the second-order smoother, we smoothed u_j^n at every 24,000 time steps ($\pi t = 12$) to compare the resulting u_j^n with those obtained from the present Runge–Kutta smoother. We found that the Runge–Kutta smoother leads to results better than those of the second-order smoother.

The present paper treats the initial monochromatic wave given by Eq. (2.4) with relatively small amplitude $\varepsilon_K = 0.25$ so that the parametric excitation of the computational modes can be analysed theoretically. We are comparing overall validities of the Runge–Kutta smoother and the second-order smoother applied to Eqs. (2.3) and (2.4) for various amplitude ε_K. We are also examining how often we need the smoothing in long-time integrations of the Korteweg–de Vries equation. The results will appear in the next paper.

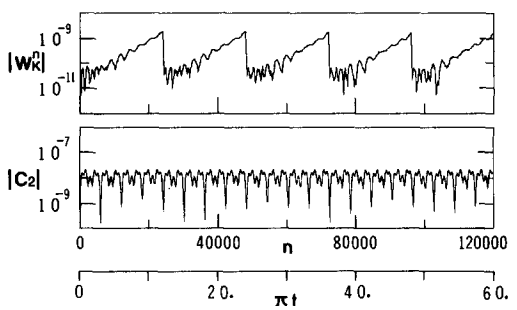

FIG. 9. Computational mode W_K^n and invariant C_2 for Fig. 1 as functions of time, when computational modes are eliminated at every 24,000 time steps ($\pi t = 12$). μ, Δt, Δx, K, and ε_K are given in Fig. 1.

7. Conclusions

(i) The numerical instability, which often occurs in the usage of the leap-frog scheme applied to the Korteweg–de Vries equation, comes from the growth of computational modes.

(ii) The computational modes are parametrically coupled with the physical modes.

(iii) The parametric excitation of the computational modes occurs only for the intermediate amplitude of wave (see Figs. 7 and 8).

(iv) Even if the amplitude of a wave is large, we can make long-time integration of the Korteweg–de Vries equation by eliminating the computational modes not at each time step, but at some time steps.

References

1. B. J. Daly, *Math. Comput.* **17**, 346 (1963).
2. C. W. Hirt, *J. Comput. Phys.* **2**, 339 (1968).
3. B. Fornberg, *Math. Comput.* **27**, 45 (1973).
4. F. Vadillo and J. M. Sanz-Serna, *J. Comput. Phys.* **66**, 225 (1986).
5. D. M. Sloan and A. R. Mitchell, *J. Comput. Phys.* **67**, 372 (1986).
6. W. L. Briggs, A. C. Newell, and T. Sarie, *J. Comput. Phys.* **51**, 83 (1983).
7. N. Yajima and T. Nogi, *Numerical Analysis of Evolution Equations* (Iwanami, Tokyo, 1977). [Japanese]
8. H. M. Hsia and Y. N. Jeng, *J. Comput. Phys.* **68**, 251 (1987).
9. N. J. Zabusky and M. D. Kruskal, *Phys. Rev. Lett.* **15**, 240 (1965).
10. C. S. Gardner, J. M. Greene, M. D. Kruskal, and R. M. Miura, *Phys. Rev. Lett.* **19**, 1095 (1967).
11. K. Abe and N. Satofuka, *Phys. Fluids* **24**, 1045 (1981).
12. N. J. Zabusky, private communication.